Nanoscale

A Novel SWCNT-Polyoxometalate Nanohybrid Material as Electrode for Electrochemical Supercapacitors

Journal:	*Nanoscale*
Manuscript ID:	NR-ART-12-2014-007528.R1
Article Type:	Paper
Date Submitted by the Author:	10-Feb-2015

Complete List of Authors:	Chen, Han-Yi; Technische Universität München, Department of Chemistry Al-Oweini, Rami; Beirut Arab University, Department of Chemistry, Faculty of Science; Jacobs University Bremen, Department of Chemistry Friedl, Jochen; Technische Universität München, Department of Physics E19 Lee, Ching Yi; Nanyang Technological University, School of Materials Science and Engineering Li, Linlin; Nanyang Technological University, School of Materials Science and Engineering Kortz, Ulrich; Jacobs University Bremen, School of Engineering and Science Stimming, Ulrich; Newcastle University, School of Chemistry, Faculty of Science, Agriculture and Engineering; Technische Universität München, Department of Physics E19; Technische Universität München, Department of Chemistry; TUM CREATE, Srinivasan, Madhavi; Nanyang Technological University, Materials Science and Engineering; TUM CREATE, ; Energy Research Institute @ NTU (ERI@N),

Nanoscale

RSCPublishing

ARTICLE

A Novel SWCNT-Polyoxometalate Nanohybrid Material as Electrode for Electrochemical Supercapacitors

Cite this: DOI: 10.1039/x0xx00000x

Received 00th January 2012,
Accepted 00th January 2012

DOI: 10.1039/x0xx00000x

www.rsc.org/

Han-Yi Chen,[a,b] Rami Al-Oweini,[c,d] Jochen Friedl,[a,e] Ching Yi Lee,[f] Linlin Li,[a,f] Ulrich Kortz,[c] Ulrich Stimming,*[a,b,e,g] and Madhavi Srinivasan*[a,f,h]

A novel nanohybrid material that combines single-walled carbon nanotubes (SWCNTs) with a polyoxometalate $(TBA)_5[PV^V_2Mo^{VI}_{10}O_{40}]$ (**TBA-PV_2Mo_{10}**, TBA: $[(CH_3(CH_2)_3)_4N]^+$, tetra-n-butyl ammonium) is investigated for the first time as electrode material for supercapacitors (SCs) in this study. The **SWCNT-TBA-PV_2Mo_{10}** material has been prepared by a simple solution method which electrostatically attaches anionic $[PV_2Mo_{10}O_{40}]^{5-}$ anions with organic TBA cations on the SWCNTs. The electrochemical performance of SWCNT-TBA-PV_2Mo_{10} electrodes is studied in acidic aqueous electrolyte (1 M H_2SO_4) by galvanostatic charge/discharge and cyclic voltammetry. In this **SWCNT-TBA-PV_2Mo_{10}** nanohybrid material, **TBA-PV_2Mo_{10}** provides redox activity while benefiting from the high electrical conductivity and high double-layer capacitance of the SWCNTs that improve both energy and power density. An assembled **SWCNT-TBA-PV_2Mo_{10}** symmetric SC exhibits a 39 % higher specific capacitance as compared to a symmetric SC only employing SWCNTs as electrode material. Furthermore, the **SWCNT-TBA-PV_2Mo_{10}** SC exhibits excellent cycling stability, retaining 95 % of its specific capacitance after 6500 cycles.

Introduction

Supercapacitors (SCs) have experienced growing interest due to increasing demand for energy storage with high power density and long cycle lifetime.[1] Such high power energy storage can be employed for portable electronics, electromobility, memory backup system, load levelling, and uninterruptible power sources.[2] SCs also provide much higher energy densities than traditional static capacitors.

The most commonly used electrode material in commercial SCs is activated carbon (AC) which provides high surface area (1000—3500 $m^2 g^{-1}$) with double layer capacitance varying from 27.9 to 140 $F g^{-1}$.[3, 4] However, activated carbon is unable to provide high power due to its low electric conductivity (10 to 100 S m^{-1})[5] which is limited by heat treatment. High temperature treatment (~ 700 °C) is required to increase their conductivity by forming conjugated sp^2 carbon during carbonization.[6] Other nanostructured carbon materials such as fullerenes,[7] carbon nanotubes (CNTs),[8] graphene,[9] and nanofibers have been developed for SCs applications. Especially CNTs with high electric conductivity (ranging from 10^3 S m^{-1} for multi-walled carbon nanotubes (MWCNTs) and to 10^8 S m^{-1} for single-walled carbon nanotubes (SWCNTs))[10, 11] and high surface area have been widely studied as electrode material for SCs. The specific capacitance of MWCNTs was reported to range from 49 to 120 $F g^{-1}$,[12-14] and the specific capacitance of SWCNTs was reported with values from 20 to 300 $F g^{-1}$.[15-18] However, all the SCs made from carbon materials suffer from low energy density due to the limited charge storage capability. Therefore, carbon materials combined with pseudocapacitive materials have been developed to achieve higher energy density.

Pseudocapacitive materials such as electroconducting polymers (ECPs), transition metal oxides (TMOs), and polyoxometalates (POMs), provide high pseudocapacitance which is caused by electrochemical redox reactions. POMs are transition metal oxide clusters with well-defined structures.[19-23] They are known to achieve high capacity for energy storage applications due to fast and reversible multi-electron redox reactions.[19-27]

In literature, some POM materials have been studied in SCs as shown in **Table 1**.[1, 25, 27-41] Due to the high solubility of those POMs in aqueous solutions, most of them were anchored onto substrates such as CNTs,[30, 31] AC,[29] or ECP[28, 31, 32, 34] to prevent the dissolution of the POMs into the aqueous electrolytes and also to increase the electrical conductivity. Most of the POMs we investigated (see Table 1) are of the keggin type, $[XV_nMo_{12-n}O_{40}]^{m-}$ (X= P or Si; n= 0–3), and they are electrochemically active and stable in the acidic,

Table 1. Summary table of supercapacitor with POM electrodes

Electrode	Electrolyte/ Membrane	Device	Current density/ scan rate	Specific capacitance	Cycle no. (retention)	Ref
$H_3PMo_{12}O_{40}//H_xRuO_2$	Nafion 117	Asymmetric device	2.2 mA cm^{-2}	112 F g^{-1}	-	27
$H_3PMo_{12}O_{40}$/PAni[a]	poly(2,5-benzimidazole)	Symmetric device	0.125 mA cm^{-2}	195 mF cm^{-2}	2000^{th} (~85%)	36
$H_3PMo_{12}O_{40}$/PAni	Nafion 117	Symmetric device	0.4 A g^{-1}	168 F g^{-1}	200^{th} (~60%)	37
$H_3PMo_{12}O_{40}$/PAni	Nafion117+acid	Symmetric device	0.4 A g^{-1}	110 F g^{-1}	4000^{th} (~68%)	34
$H_3PMo_{12}O_{40}$/PPy[b]	0.1 M H_2SO_4	3-electrode configuration	1 mV s^{-1}	130 F g^{-1}	-	32
$H_3PMo_{12}O_{40}$/PPy	Nafion 115	3-electrode configuration	1 mV s^{-1}	22.9 F g^{-1}	-	38
$H_5PV_2Mo_{10}O_{40}$/PPy	0.1 M H_2SO_4	3-electrode configuration	1 mV s^{-1}	422 F g^{-1}	-	32
$H_5PV_2Mo_{10}O_{40}$/PPy	Nafion 115	3-electrode configuration	1 mV s^{-1}	27.6 F g^{-1}	-	38
$H_4SiMo_{12}O_{40}$/PPy	0.1 M H_2SO_4	3-electrode configuration	1 mV s^{-1}	266 F g^{-1}	-	32
$H_4SiMo_{12}O_{40}$/PPy	Nafion 115	3-electrode configuration	1 mV s^{-1}	33.4 F g^{-1}	-	38
$H_3PMo_{12}O_{40}$/PPy// $H_3PW_{12}O_{40}$/PEDOT[c]	0.5 M H_2SO_4	Asymmetric device	1 mA	31 F g^{-1}	200^{th} (~68%)	33
$H_3PMo_{12}O_{40}$/PEDOT	0.1 M H_2SO_4	3-electrode configuration	10 mV s^{-1}	140 F g^{-1}	-	28
$H_5PV_2Mo_{10}O_{40}$/PEDOT	0.1 M H_2SO_4	3-electrode configuration	10 mV s^{-1}	70 F g^{-1}	-	28
$Cs_xPMo_{12}O_{40}$/MWCNT	Nafion 117+acid	Symmetric device	0.2 A g^{-1}	285 F g^{-1}	500^{th} (~65%)	30
$H_3PMo_{12}O_{40}$/MWCNT	1 M H_2SO_4	Symmetric device	1 A g^{-1}	38 F g^{-1}	-	1
$H_3PMo_{12}O_{40}$/PDDA/ Carbon Nanoparticles	1 M H_2SO_4	3-electrode configuration	5 V s^{-1}	0.6 F cm^{-2}	-	25
$H_3PMo_{12}O_{40}$/PDDA[d]/ MWCNT	1 M H_2SO_4	3-electrode configuration	50 mV s^{-1}	2.68 F cm^{-2}	-	31
$H_3PMo_{12}O_{40}$/PDDA/ MWCNT	1 M H_2SO_4	3-electrode configuration	50 mV s^{-1}	1.93 F cm^{-2}	-	31
$H_3PMo_{12}O_{40}$+$H_4SiMo_{12}O_{40}$/ PDDA/MWCNT	1 M H_2SO_4	3-electrode configuration	10 mV s^{-1}	2.4 F cm^{-2}	-	39
$H_3PMo_{12}O_{40}$+$H_5PV_2Mo_{10}O_{40}$/ PDDA/MWCNT	1 M H_2SO_4	3-electrode configuration	50 mV s^{-1}	158 F cm^{-3}	-	40, 41
$H_3PMo_{12}O_{40}$/AC	1 M H_2SO_4	Symmetric device	1 A g^{-1}	140 F g^{-1}	8000^{th} (~91%)	29
$Na_6V_{10}O_{28}$//AC	1 M $LiClO_4$	Asymmetric device	0.1 A g^{-1}	354 F g^{-1}	1000^{th} (~70%)	35

[a] PAni: polyaniline [b] PPy: polypyrrole [c] PEDOT: poly(3,4-ethylenedioxythiophene) [d] PDDA: poly(diallyldimethylammonium) chloride

aqueous electrolytes used here. [1, 25, 28, 29, 31-33, 39-41]

So far two methods have been utilized to prepare POM/Carbon hybrid materials for SCs: sonication and layer-by-layer (LbL) deposition.[1, 25, 29-31] Ruiz et al. prepared an AC/PMo_{12} hybrid material by sonicating a POM solution with AC powder, which led to adsorption of the POM onto the surface of AC. This AC/PMo_{12} symmetric SC provided a specific capacitance of 183 F g^{-1} at current density of 2 A g^{-1}.[29] MWCNTs/POM hybrid materials as electrode materials for symmetric SCs were also prepared by sonication method followed by several purification steps.[1, 30] MWCNTs/PMo_{12} hybrid materials reported by Skunik et al. provided specific capacitance of 40 F g^{-1} at a current of 7 mA,[1] and MWCNTs/Cs-PMo_{12} hybrid materials reported by Cuentas-Gallegos et al. showed high specific capacitance of 285 F g^{-1} at a current density of 0.2 A g^{-1}, but only 20 F g^{-1} at current density of 2 A g^{-1}.[30] Single POM molecules are usually adsorbed at defect sites and form

monolayers.[1, 30] Excess POM molecules are washed out due to the high solubility in aqueous solution and the amount of chemisorbed POMs is also dependent on the functionalization degree of the carbon materials.[1, 30]

The LbL deposition method provides a simpler way to prepare POM/Carbon hybrid material by alternating electrostatic adsorption of cationic polymer (ex. poly(diallyldimethylammonium) chloride, PDDA) and anionic POMs on functionalized carbon materials.[25, 31, 39] However, the long polymer chain might restrict electron hopping from POM to SWCNT.

In this study, we present for the first time the combination of SWCNTs and $(TBA)_5[PV_2Mo_{10}O_{40}]$ (**TBA-PV_2Mo_{10}**, TBA: $[(CH_3(CH_2)_3)_4N]^+$, tetra-n-butyl ammonium), as electrode material for SCs in acidic aqueous electrolyte (1 M H_2SO_4). Unlike other POMs used in SCs, **TBA-PV_2Mo_{10}** is insoluble in aqueous electrolyte due to its organic cation (TBA). Therefore, high cycling stability in acidic aqueous electrolyte is expected. Purified SWCNTs with 1−3 atomic% carboxylic acid groups are employed in this study. The hydrophilic carboxylic acid groups enhance the contact with polar aqueous electrolytes, and also provide pseudocapacitance. The anionic $[PV_2Mo_{10}O_{40}]^{5-}$ are electrostatically attached to the SWCNTs through the organic TBA cations. Thus, **SWCNT-TBA-PV_2Mo_{10}** nanohybrid material can be prepared by an even simpler solution process than sonication and LbL methods. TBA has much shorter alkyl chains than cationic polymers,[25, 31, 39] which also shortens the electron-hoping distance between POMs and SWCNTs. The idea of **SWCNT-TBA-PV_2Mo_{10}** is combining double-layer capacitance, mainly contributed from SWCNTs, and pseudocapacitance mainly contributed from **TBA-PV_2Mo_{10}**. **TBA-PV_2Mo_{10}** provides redox activity while benefiting from the conducting properties of the SWCNTs that improve both energy and power density.

Results and discussion

Material characterization of TBA-PV_2Mo_{10}

The synthesized **TBA-PV_2Mo_{10}** is characterized by ^{31}P nuclear magnetic resonance (NMR), ^{51}V NMR, Fourier transform infrared spectroscopy (FTIR), and UV-Vis spectroscopy. The phosphorous and vanadium atoms in the $[PV_2Mo_{10}O_{40}]^{5-}$ structure can be detected by ^{31}P NMR and ^{51}V NMR in solution. As shown in **Figure 1a** and **1b**, the spectra show the characteristic signals of $[PV_2Mo_{10}O_{40}]^{5-}$ (^{31}P NMR: δ −2.2 ppm, −1.6 ppm; ^{51}V NMR: δ −532 ppm, −544 ppm, −551 ppm, and −554 ppm) which are similar to previous studies.[42]

Figure 1c presents the FTIR spectrum of **TBA-PV_2Mo_{10}**. The FTIR characteristic absorption bands at about 1055 cm^{-1}, 952 cm^{-1}, 880 cm^{-1}, and 802 cm^{-1} can be assigned to P-O, M=O (M: Mo, V), inter-octahedral M−O−M, and intra-octahedral M−O−M vibrations, respectively, as reported for the Keggin unit in previous studies.[43-47] The absorption bands located at 1381 and 1483 cm^{-1} can be assigned to C−H bending bond which is contributed from TBA ($[(CH_3(CH_2)_3)_4N]^{5+}$). The inset of **Figure 1c** shows the representation of **TBA-PV_2Mo_{10}**. An UV-Vis spectrum of **TBA-PV_2Mo_{10}** has been recorded and is shown in **Figure 1d.** The

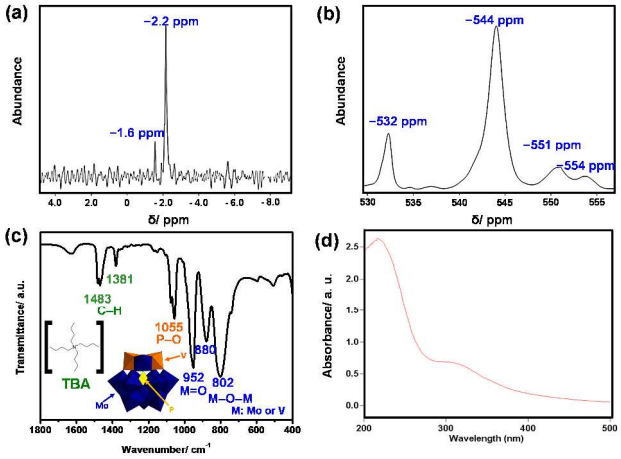

Figure 1. (a) ^{31}P NMR spectrum, (b) ^{51}V NMR spectrum, (c) FTIR spectrum, and (d) UV-Vis spectrum of **TBA-PV_2Mo_{10}**. Inset in (c) is the representation of **TBA-PV_2Mo_{10}**.

absorption band observed at 305 nm is attributed to Mo^{6+} in octahedral position at a ligand metal charge transfer state.[43]

Material characterization of SWCNT-TBA-PV_2Mo_{10} material

The **SWCNT-TBA-PV_2Mo_{10}** material was prepared by a simple solution method. A suspension of SWCNTs and **TBA-PV_2Mo_{10}** in acetonitrile solution was stirred for 10 min as described in the experimental section. **SWCNT-TBA-PV_2Mo_{10}** nanohybrid material is not restricted to form monolayers of POM onto SWCNTs due to the insoluble nature of **TBA-PV_2Mo_{10}** in aqueous electrolyte. Thus, the amount of **TBA-PV_2Mo_{10}** in the nanohybrid material can be optimized. By varying the precursor weight ratio of SWCNTs and **TBA-PV_2Mo_{10}**, the optimum precursor weight ratio was determined to be 30 wt % **TBA-PV_2Mo_{10}** and 70 wt % SWCNTs. After synthesis the weight ratio of **TBA-PV_2Mo_{10}** in **SWCNT-TBA-PV_2Mo_{10}** material was determined to be around 30 wt % by thermogravimetric analysis (TGA) analysis (**Figure 2a)**, indicating that all **TBA-PV_2Mo_{10}** molecules are attached to SWCNTs.

Figure 2b shows the FTIR spectra of SWCNT, **TBA-PV_2Mo_{10}**, and **SWCNT-TBA-PV_2Mo_{10}**. The vibrational modes of $[PV_2Mo_{10}O_{40}]^{5-}$ polyanion (P-O: 1055 cm^{-1}, M=O: 952 cm^{-1}, and M−O−M: 880, 802 cm^{-1}) remain in the nanohybrid material, representing the combination of POM and SWCNT.

A Brunauer-Emmett-Teller (BET) measurement of the surface areas is obtained for SWCNT, **TBA-PV_2Mo_{10}**, and **SWCNT-TBA-PV_2Mo_{10}** by N_2 adsorption-desorption isotherms as shown in **Figure 2c**. The surface areas of SWCNT, **TBA-PV_2Mo_{10}**, and **SWCNT-TBA-PV_2Mo_{10}** are 157, 5, and 71 m^2 g^{-1}, respectively. The much higher surface area of the **SWCNT-TBA-PV_2Mo_{10}** compared to pure **TBA-PV_2Mo_{10}** is mainly attributed to SWCNTs. This indicates that the SWCNT-matrix helps the dispersion of the **TBA-PV_2Mo_{10}**

on a larger interface area, and shows the possibility of this nanohybrid material to deliver substantial double layer capacitance.

A high resolution transmission electron microscopy (HRTEM) image of as-received SWCNTs is shown in **Figure 3a.** The average

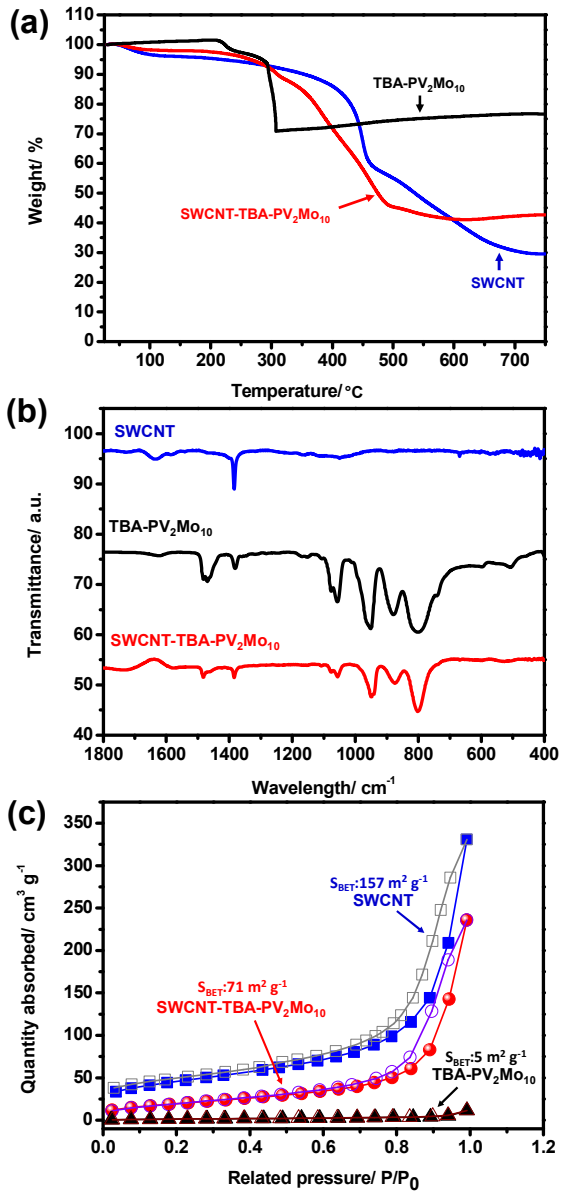

Figure 2. (a) TGA analyses, (b) FTIR spectrum, and (c) BET graph of SWCNT, **TBA-PV_2Mo_{10}**, and **SWCNT-TBA-PV_2Mo_{10}** nanohybrid

diameter of one individual tube is ~ 1.4 nm. SWCNTs tend to occur as bundles with average bundle diameters of 4-10 nm. **Figure 3b** and **3c** show a scanning electron microscopy (SEM) image and a bright-field TEM image of **SWCNT-TBA-PV_2Mo_{10}** nanohybrid material. The **TBA-PV_2Mo_{10}** recrystallizes on the surface of the SWCNTs, showing nanoparticle agglomerates with a diameter of 20–500 nm. The SWCNTs link those POM nanoparticles together and form an electrically conductive network. Furthermore, nano-sized black spots with a diameter around 1.5 nm are grafted on the surface of SWCNTs separately as shown in the TEM image, and they can be considered to be **TBA-PV_2Mo_{10}** single molecules.[26] For clarity, they

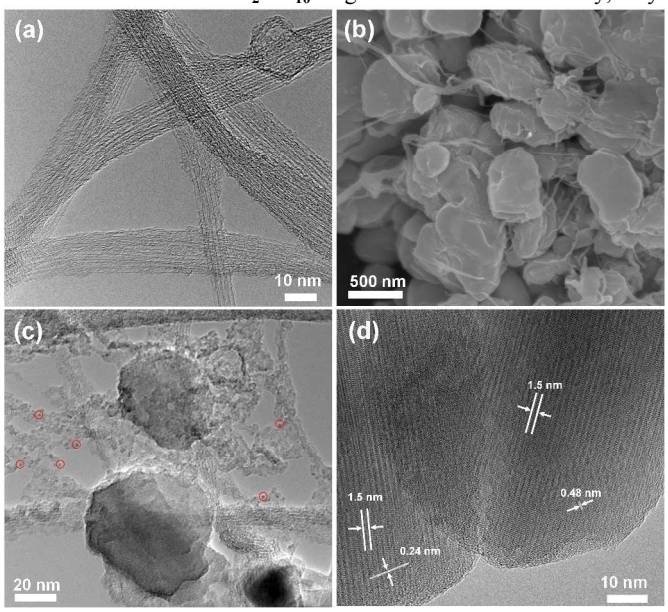

Figure 3. (a) HRTEM image of as received SWCNTs. (b) SEM image, (c) the bright-field TEM image, and (d) HRTEM image of **SWCNT-TBA-PV_2Mo_{10}** nanohybrid

are highlighted with red circles. The HRTEM image provides further insights into the crystal structure of the **TBA-PV_2Mo_{10}** nanoparticles as shown in **Figure 3d**. The d-spacings of the **TBA-PV_2Mo_{10}** nanoparticles are 1.5 nm, 0.48 nm, and 0.24 nm; they exhibt polycrystallinity in random orientation.

Electrochemical performance of SWCNT-TBA-PV_2Mo_{10} electrode

In order to investigate the electrochemical performance and pseudocapacitive behavior of **SWCNT-TBA-PV_2Mo_{10}** nanohybrid material as electrode material for SCs, three-electrode cyclic voltammetry (CV) was performed. A Pt wire served as the counter electrode while Ag/AgCl (in 3.5 M KCl) was employed as the reference electrode. **Figure 4a** shows the CV curves of blank (polished glassy carbon with a diameter of 5 mm), **TBA-PV_2Mo_{10}**, SWCNT, and **SWCNT-TBA-PV_2Mo_{10}** electrodes measured from −0.2 V to 1.0 V vs. Ag/AgCl at scan rates of 10 mV s^{-1}. The current generated from the blank electrode is negligible. The CV curve of the SWCNT electrode shows a rectangular double-layer capacitive behavior with a couple of broad redox peaks at the potential range of 0.3−0.5 V vs. Ag/AgCl, which stem from the faradic reactions of carboxylic acid groups on the surface of SWCNTs.[1] The CV curves of **TBA-PV_2Mo_{10}** electrode deviate from the rectangular shape of an ideal capacitor showing faradaic processes (pseudocapacitance).[35] The redox peaks of **TBA-PV_2Mo_{10}** electrode are broad and not well-defined due to the low electrical conductivity. The CV curve of **SWCNT-TBA-PV_2Mo_{10}** electrode deviates from the curve of

SWCNT electrode and shows four well-defined redox peaks, which are similar with the redox peaks observed in **TBA-PV_2Mo_{10}** electrode, indicating a combination of double-layer capacitance mainly contributed from SWCNT and pseudocapacitance mainly contributed from **TBA-PV_2Mo_{10}**.[29] The main oxidation peaks can be observed at (i) 0.48 V, (ii) 0.37 V, (iii) 0.23 V, and (iv) −0.03 V vs. Ag/AgCl, corresponding reduction peaks are located at (i') 0.45, (ii') 0.30 V, (iii') 0.20 V, and (iv') −0.06 V vs. Ag/AgCl. A small oxidation peak (labeled as *) is observed at 0.1 V vs. Ag/AgCl which might be an intermediate reaction of (iii). A couple of peaks labeled with circles at −0.15 and −0.2 V vs. Ag/AgCl are irreversible reactions which will not be discussed here. The redox couples of ii/ii', iii/iii', and iv/iv' are two-electron reversible systems, which are contributed from the redox reaction of Mo atoms. The redox couple of i/i' with a more positive potential than the other three reactions can be ascribed to the redox reaction of V atoms and also the faradic reactions of carboxylic acid groups on the surface of SWCNTs. The electrochemical behavior of $[PV_2Mo_{10}O_{40}]^{5-}$ resembles studies reported by Barth and Bajwa et.al. [36, 37] According to literature, the redox reactions of $[PV_2Mo_{10}O_{40}]^{5-}$ can be summarized by the following equations:[32, 41, 48]

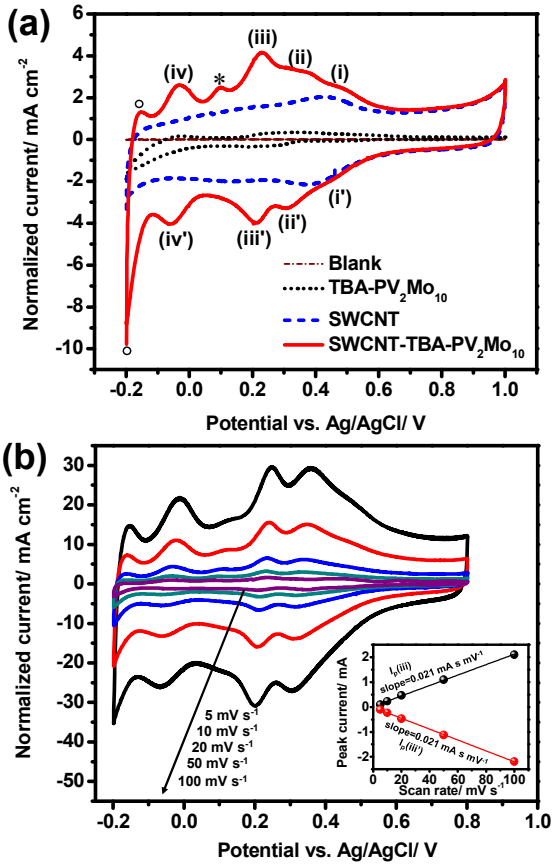

Figure 4. Cyclic voltammograms of (a) blank (glassy carbon), **TBA-PV_2Mo_{10}**, SWCNT, and **SWCNT-TBA-PV_2Mo_{10}** electrodes at 10 mV s^{-1}, and (b) **SWCNT-TBA-PV_2Mo_{10}** electrodes at 100, 50, 20, 10, 5 mV s^{-1} in 1 M H_2SO_4 in a three-electrode configuration with Pt wire as the counter electrode and Ag/AgCl as the reference electrode. Inset in (b) is peak current versus scan rate for the process (iii/iii´).

$$[PV_2^V Mo_{10}^{VI} O_{40}]^{5-} + (6+n)e^- + (6+n)H^+ \leftrightarrow H_{6+n}[PV_{2-n}^V V_n^{IV} Mo_6^{VI} Mo_4^V O_{40}]^{5-} \quad (1)$$

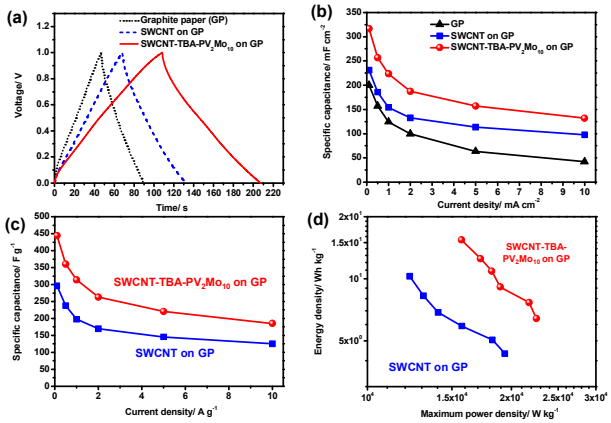

Figure 5. Electrochemical performance of SWCNT and **SWCNT-TBA-PV_2Mo_{10}** symmetric SC. (a) Galvanostatic charge-discharge curves at current densities of 1 mA cm^{-2}. (b) The specific capacitance normalized by area at current densities of 0.1-10 mA cm^{-2}. (c) The specific capacitance and (d) the Ragone plots normalized by mass at various current densities of 0.1-10 A g^{-1}.

CV curves of the SWCNT-TBA-PV_2Mo_{10} electrode at various scan rates ranging from 5 to 100 mV s^{-1} are shown in **Figure 4b**. The relation between peak currents (I_p) and scan rates (ν) for process iii/iii´ are illustrated in the inset of **Figure 4b**, and those data points generate two straight lines with slopes that have the same absolute slope. The peak current is proportional to the scan rate indicating that the redox-processes are surface-processes and are not diffusion controlled ($I_p \propto \nu^{0.5}$).[29, 49, 50] The other three redox processes also shows a similar behavior. The relationship of peak current and scan rate can be expressed by following equation:[29]

$$I_p = \frac{n^2 F^2 A \Gamma \nu}{4RT} \quad (2)$$

where n is number of electrons, F is Faraday's constant, A is the surface area measured from BET (cm^2), Γ is surface coverage (mol cm^{-2}), R is ideal gas constant, and T is temperature (K). The surface coverage of SWCNT-TBA-PV_2Mo_{10} electrode can be calculated from eq. (2): $\Gamma = 1.8 \times 10^{-11}$ mol cm^{-2}. Comparing this to the maximum theoretical value (1.4×10^{-10} mol cm^{-2}), which assumes full coverage of Keggin-type POMs onto a flat accessible surface such as graphite,[29, 51] the lower surface coverage value of **SWCNT-TBA-PV_2Mo_{10}** electrode indicates that the pore accessibility is limited.

Symmetric SCs are assembled to demonstrate the potential of **SWCNT-TBA-PV_2Mo_{10}** electrodes for actual device applications. The commonly used current collector, graphite paper (GP), was employed in these SC devices. However, the current generated from

GP cannot be ignored in acidic aqueous electrolyte. Thus, we calculated the specific capacitance normalized to both the geometric working area as well as the mass. **Figure 5a** shows the galvanostatic charge/discharge curves of GP, SWCNT, and **SWCNT-TBA-PV_2Mo_{10}** symmetric SCs at current densities of 1 A g^{-1} (mass based on single electrode) in 1 M H_2SO_4. The linear charge/discharge curve of blank electrode (GP) and SWCNT symmetric SC represents ideally double-layer capacitive behaviour. The slope of the charge/discharge curve of **SWCNT-TBA-PV_2Mo_{10}** symmetric SC is not strictly linear, showing a combination of double-layer capacitance and pseudocapacitance. The specific capacitance (C_{sp}) of a symmetric SC can be calculated using the following equation:[1]

$$C_{sp}^{A} = \frac{2C}{A} \; or \; C_{sp}^{m} = \frac{2C}{m} \quad (3)$$

where A is the geometric surface area, m is the mass of the active materials (SWCNT or **SWCNT-TBA-PV_2Mo_{10}**) in one electrode, and C is the experimental capacitance obtained using the following equation:[1, 29]

$$C = \frac{I}{(\frac{dV}{dt})} \quad (4)$$

where I is the constant current, V is the potential range, and t is discharge time, respectively.

Figure 5b compares the specific capacitance defined in terms of geometric surface area of GP blank electrodes (thickness: 195.3±1.8 μm, areal density: ~ 22 mg cm^{-2}), SWCNT (film thickness: 39.7 ± 3.8 μm, areal density: ~ 1 mg cm^{-2}), and **SWCNT-TBA-PV_2Mo_{10}** (film thickness: ~ 30.7 ± 2.8 μm, areal density: ~ 1 mg cm^{-2}) at various current densities from 10 to 0.1 mA cm^{-2}. Although the specific capacitance of GP defined in term of geometric working area is significant in acidic aqueous electrolyte, there is improvement contributed from **SWCNT-TBA-PV_2Mo_{10}** material. The **SWCNT-TBA-PV_2Mo_{10}** symmetric SC provides a specific capacitance of 132, 157, 187, 224, 256, and 317 mF cm^{-2} at current densities of 10, 5, 2, 1, 0.5, and 0.1 mA cm^{-2}, respectively. This represents a much higher specific capacitance than the SWCNT symmetric SC (the specific capacitances are 98, 113, 132, 154, 186, and 231 mF cm^{-2} at current densities of 10, 5, 2, 1, 0.5, and 0.1 mA cm^{-2}, respectively). A 39 % higher specific capacitance is obtained in average. The increase of specific capacitance is a result of the pseudocapacitive contribution of **TBA-PV_2Mo_{10}** in the nanohybrid.[30] As expected, the specific capacitances are larger at lower current densities for both SWCNT and **SWCNT-TBA-PV_2Mo_{10}** symmetric SCs.[34] The specific capacitance of SWCNT symmetric SC reduces rapidly at high current density because of the mass transfer limitation of electrolyte ions inside the porous of SWCNTs. The specific capacitance of **SWCNT-TBA-PV_2Mo_{10}** symmetric SC decreases even faster with the increasing current density, which is due to the high electrical resistance of **TBA-PV_2Mo_{10}**.[25]

The specific capacitances, energy and power densities normalized to the mass of the active material (SWCNT and **SWCNT-TBA-PV_2Mo_{10}**) at various current densities from 10 to 0.1 A g^{-1} are also shown in **Figure 5c** and **5d**, respectively. At high current density of 10 A g^{-1}, the **SWCNT-TBA-PV_2Mo_{10}** symmetric SC provides a specific capacitance of 185 F g^{-1} while SWCNT symmetric SC provides 125 F g^{-1}. The **SWCNT-TBA-PV_2Mo_{10}** symmetric SC exhibits a much higher specific capacitance of 444 F g^{-1} at current densities of 0.1 A g^{-1}, while the specific capacitance of SWCNT symmetric SC is only 236 F g^{-1}.

Energy and maximum power densities can be obtained from the following equations: [52, 53]

$$E = \frac{1}{2}\frac{C}{M}\Delta V^2 \quad (5)$$

$$P_{max} = \frac{\Delta V^2}{4RM} \quad (6)$$

where M is the total mass of the active material in both negative and positive electrodes (kg), and R is the device resistance (Ω). It can be observed in the Ragone plots that **SWCNT-TBA-PV_2Mo_{10}** symmetric SC delivers higher energy density than SWCNT symmetric SC at the same power density. The maximum energy density of 15.4 Wh kg^{-1} can be obtained from the **SWCNT-TBA-PV_2Mo_{10}** symmetric SC with a power density of 15.7 kW kg^{-1}, whereas the energy density of SWCNT symmetric SC is around 6 Wh kg^{-1} at a similar power density. Even at a high power density of 22.5 kW kg^{-1}, the energy density of **SWCNT-TBA-PV_2Mo_{10}** symmetric SC still provides higher energy density of 6.4 Wh kg^{-1} than SWCNT symmetric SC. Those results demonstrate that **SWCNT-TBA-PV_2Mo_{10}** symmetric SC in acidic aqueous electrolyte is promising for high power SC applications. However, it should be noted those SC devices were tested so far only on a small lab scale.

The capacitance retention of **SWCNT-TBA-PV_2Mo_{10}** symmetric SC measured in cycling charge-discharge test at current density of 1 A g^{-1} is shown in **Figure 6**. After 6500 cycles, the **SWCNT-TBA-PV_2Mo_{10}** symmetric SC exhibits excellent cycle stability with a capacitance retention of ~ 95 %. This high cycle stability is mainly contributed by the insoluble nature of **TBA-PV_2Mo_{10}**. Compared to other POM SCs with 2-electrode configuration (both symmetric and asymmetric devices) shown in Table 1, the **SWCNT-TBA-PV_2Mo_{10}** symmetric SC in this study exhibits the highest stability and capacitance (normalized to the mass of the active materials).

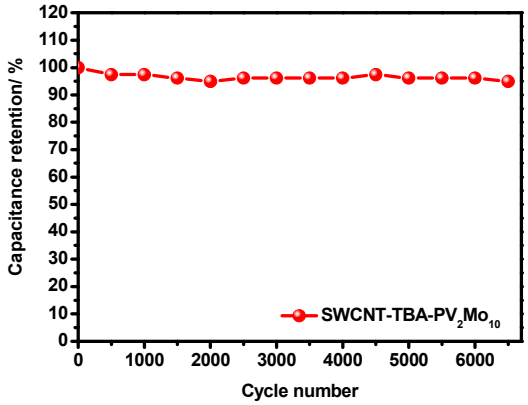

Figure 6. Capacitance degradation of **SWCNT-TBA-PV_2Mo_{10}** symmetric SC at current densities of 1 A g^{-1}.

Conclusions

In summary, a **SWCNT-TBA-PV_2Mo_{10}** nanohybrid material has been successfully synthesized in a simple solution process and has been demonstrated to be a promising electrode material for SCs for the first time. The **SWCNT-TBA-PV_2Mo_{10}** symmetric SC exhibits high specific capacitance of 444 F g^{-1}, high energy density of 15.4 Wh kg^{-1} with high maximum power density of 15.7 W kg^{-1} in 1 M H_2SO_4 electrolyte. Furthermore, the **SWCNT-TBA-PV_2Mo_{10}** symmetric SC displays excellent long cycle life with capacitance retention of ~ 95 % after 6500 cycles. These encouraging findings have proofed the potential of **SWCNT-TBA-PV_2Mo_{10}** material as a promising electrode candidate for SCs with high energy density, high power density, and long cycle lifetime.

Experimental

Preparation of TBA-PV_2Mo_{10}: $[(CH_3(CH_2)_3)_4N]_5[PV_2Mo_{10}O_{40}]$ (**TBA-PV_2Mo_{10}**, TBA: $[(CH_3(CH_2)_3)_4N]^+$, tetra-n-butyl ammonium) was prepared using a literature method.[44, 54] 24.4 g sodium metavanadate ($NaVO_3$) was dissolved by 100 mL boiling H_2O, and then added to 7.1 g Na_2HPO_4 in 100 mL H_2O. After the solution cooled to room temperature, 5 mL concentrated H_2SO_4 was added, then 121 g Na_2MoO_4•$2H_2O$ in 200 mL H_2O were added and stirred vigorously. 85 mL concentrated H_2SO_4 were slowly added in the solution. 19.5 g of TBA-Br was added to the homogeneous solution to obtain orange $(TBA)_5[PV_2Mo_{10}O_{40}]$, which was thoroughly washed with water and filtered to obtain the desired powder. The identity of **TBA-PV_2Mo_{10}** was established by ^{31}P NMR, ^{51}V NMR, FTIR, and UV-Vis spectra. The NMR spectra were recorded on a 400 MHz JEOL ECX instrument. FTIR spectrophotometer (PerkinElmer Frontier FT-IR) was used to detect the infrared spectra using KBr pellets. UV-Vis spectroscopy was carried out on a UV-Vis spectrophotometer (Varian Cary 100 Bio).

Preparation of SWCNT-TBA-PV_2Mo_{10} nanohybrid: Purified SWCNTs with 1−3 atomic% carboxylic acid groups were purchased from Carbon Solution, Inc. The **SWCNT-TBA-PV_2Mo_{10}** nanohybrid material was prepared using a literature method.[26] 17 mg of **TBA-PV_2Mo_{10}** was dissolved in acetonitrile solution (5 mL), and was then added to a toluene suspension (50 mL) with 40 mg purified SWCNTs. The yellowish mixture was stirred vigorously at room temperature for 10 minutes. After leaving the mixture to stand for 1 hour, the solution became colorless and black precipitate was formed which almost indicates that all the **TBA-PV_2Mo_{10}** molecules were grafted onto the surface of SWCNTs. The precipitation was obtained by filtering the solution using a membrane with pore diameter of 0.1 mm, and then was washed with toluene for several times. Finally, the obtained precipitate was dried at 80 °C under vacuum overnight. Thermogravimetric analysis (TGA) of SWCNT, **TBA-PV_2Mo_{10}**, and **SWCNT-TBA-PV_2Mo_{10}** was recorded on a TA Instruments SDT Q600 thermobalance with 100 mL min^{-1} flow of argon and the temperature was increased from 20 to 750 °C at a rate of 5 °C min^{-1}. The Brunauer Emmetand Teller (BET) surface area of **SWCNT-TBA-PV_2Mo_{10}**, SWCNT, and **TBA-PV_2Mo_{10}** were determined by N_2 adsorption-desorption isotherms at 77 K. The morphology of the **SWCNT-TBA-PV_2Mo_{10}** was characterized by field emission scanning electron microscope (FESEM, JEOL JSM 7600F) and high resolution transmission electron microscopy (HRTEM, JOEL-JSM 2010F).

Electrochemical measurement: The active layers of electrodes were prepared by mixing active material (**SWCNT-TBA-PV_2Mo_{10}**, SWCNT, or **TBA-PV_2Mo_{10}**), poly(vinylidene fluoride) (PVDF) binder, and carbon black (super P) in N-methylpyrrolidinone (NMP) with a weight ratio of 75 : 15 : 10, respectively. The slurry was coated onto the facets of glassy carbon rods and graphite papers as working electrodes, and dried at 80 °C overnight. The film thickness was determined by digimatic micrometer. An acidic aqueous electrolyte (1 M H_2SO_4) was used as electrolyte. Cyclic voltammetry (CV) of **SWCNT-TBA-PV_2Mo_{10}** nanohybrid material and SWCNT coated on glassy carbon electrodes was performed using a three-electrode cell. Potential and current control and data acquisition was done with a Biologic VMP3 potentiostat. Ag/AgCl in 3.5 M KCl was used as the reference electrode, and platinum wire was used as the counter electrode. The symmetric devices were fabricated using graphite papers as current collector, and porous glassy fibrous papers (GF/D) purchased from Whatman as separators. The symmetric devices were characterized by galvanostatic charge/discharge cycle measurements with a potentiostat (Solatron, SI 1255B) in the potential range of 0–1 V.

Acknowledgements

This work was supported by TUM CREATE which is a joint research programme between Technische Universität München (TUM) in Germany and Nanyang Technological University (NTU) in Singapore with partial funding by the National Research Foundation of Singapore.

Notes and references

[a] TUM CREATE, 1 CREATE Way, #10-02 CREATE Tower, 138602 Singapore
[b] Department of Chemistry, Technische Universität München, Lichtenbergstraße 4, 85748 Garching, Germany
[c] School of Engineering and Science, Jacobs University, P.O. Box 750561, 28725 Bremen, Germany
[d] Department of Chemistry, Faculty of Science, Beirut Arab University, P.O. Box 11 50 20, Riad El Solh 1107 2809, Beirut, Lebanon
[e] Department of Physics E19, Technische Universität München James-Franck Str. 1, 85748 Garching, Germany
[f] School of Materials Science and Engineering, Nanyang Technological University, 639798 Singapore
[g] School of Chemistry, Faculty of Science, Agriculture and Engineering, Bedson Building, Newcastle University, Newcastle upon Tyne NE1 7RU, United Kingdom

[h] Energy Research Institute @ NTU (ERI@N), Research Techno Plaza, 50 Nanyang Drive, 637553 Singapore
*E-mail: madhavi@ntu.edu.sg, Ulrich.Stimming@newcastle.ac.uk

1. M. Skunik, M. Chojak, I. A. Rutkowska and P. J. Kulesza, *Electrochim. Acta*, 2008, **53**, 3862.
2. G. L. Soloveichik, *Annu. Rev. Chem. Biomol. Eng.*, 2011, **2**, 503.
3. P. Simon and Y. Gogotsi, *Nat. Mater.*, 2008, **7**, 845.
4. E. Frackowiak and F. Beguin, *Carbon*, 2001, **39**, 937.
5. M. F. El-Kady, V. Strong, S. Dubin and R. B. Kaner, *Science*, 2012, **335**, 1326.
6. A. G. Pandolfo and A. F. Hollenkamp, *J. Power Sources*, 2006, **157**, 11.
7. M. Egashira, S. Okada, Y. Korai, J. Yamaki and I. Mochida, *J. Power Sources*, 2005, **148**, 116.
8. C. Portet, G. Yushin and Y. Gogotsi, *Carbon*, 2007, **45**, 2511.
9. M. D. Stoller, S. J. Park, Y. W. Zhu, J. H. An and R. S. Ruoff, *Nano Lett.*, 2008, **8**, 3498.
10. G. T. Pham, Y. B. Park, Z. Liang, C. Zhang and B. Wang, *Composites Part B*, 2008, **39**, 209.
11. Y. L. Yang, Y. D. Wang, Y. Ren, C. S. He, J. N. Deng, J. Nan, J. G. Chen and L. Zuo, *Mater. Lett.*, 2008, **62**, 47.
12. C. M. Niu, E. K. Sichel, R. Hoch, D. Moy and H. Tennent, *Appl. Phys. Lett.*, 1997, **70**, 1480.
13. R. Z. Ma, J. Liang, B. Q. Wei, B. Zhang, C. L. Xu and D. H. Wu, *J. Power Sources*, 1999, **84**, 126.
14. E. Frackowiak, K. Jurewicz, S. Delpeux and F. Beguin, *J. Power Sources*, 2001, **97-8**, 822.
15. C. Y. Liu, A. J. Bard, F. Wudl, I. Weitz and J. R. Heath, *Electrochem. Solid-State Lett.*, 1999, **2**, 577.
16. J. N. Barisci, G. G. Wallace and R. H. Baughman, *Electrochim. Acta*, 2000, **46**, 509.
17. K. H. An, W. S. Kim, Y. S. Park, Y. C. Choi, S. M. Lee, D. C. Chung, D. J. Bae, S. C. Lim and Y. H. Lee, *Adv. Mater.*, 2001, **13**, 497.
18. C. G. Liu, H. T. Fang, F. Li, M. Liu and H. M. Cheng, *J. Power Sources*, 2006, **160**, 758.
19. M. T. Pope and A. Muller, *Angew. Chem. Int. Ed.*, 1991, **30**, 34.
20. U. Kortz, ed., *Issue dedicated to Polyoxometalates, Eur. J. Inorg. Chem.,* 2009, **34**, 5056.
21. Polyoxometalates in *Encyclopedia of Inorganic and Bioinorganic Chemistry* (Eds.: M. T. Pope, U. Kortz), Wiley, Washington, 2012.
22. M. T. Pope, A. Müller in *Polyoxometalate Chemistry: From Topology via Self-Assembly to Applications* (Eds.: M. T. Pope, A. M ller), Springer, Dordrecht, 2001, pp. 1.
23. C. L. Hill, *Chem. Rev.* 1998, **98**, 1.
24. M. A. Schwegler, P. Vinke, M. Vandereijk and H. Vanbekkum, *Appl. Catal., A*, 1992, **80**, 41.
25. S. Park, K. Lian and Y. Gogotsi, *J. Electrochem. Soc.*, 2009, **156**, A921.
26. N. Kawasaki, H. Wang, R. Nakanishi, S. Hamanaka, R. Kitaura, H. Shinohara, T. Yokoyama, H. Yoshikawa and K. Awaga, *Angew. Chem. Int. Ed.*, 2011, **50**, 3471.
27. A. Yamada and J. B. Goodenough, *J. Electrochem. Soc.*, 1998, **145**, 737.
28. A. M. White and R. C. T. Slade, *Electrochim. Acta*, 2004, **49**, 861.
29. V. Ruiz, J. Suarez-Guevara and P. Gomez-Romero, *Electrochem. Commun.*, 2012, **24**, 35.
30. A. Cuentas-Gallegos, R. Martinez-Rosales, M. Baibarac, P. Gomez-Romero and M. E. Rincon, *Electrochem. Commun.*, 2007, **9**, 2088.
31. T. Akter, K. W. Hu and K. Lian, *Electrochim. Acta*, 2011, **56**, 4966.
32. A. M. White and R. C. T. Slade, *Electrochim. Acta*, 2003, **48**, 2583.
33. G. M. Suppes, C. G. Cameron and M. S. Freund, *J. Electrochem. Soc.*, 2010, **157**, A1030.
34. A. K. Cuentas-Gallegos, M. Lira-Cantu, N. Casan-Pastor and P. Gomez-Romero, *Adv. Funct. Mater.*, 2005, **15**, 1125.
35. H.-Y. Chen, G. Wee, R. Al-Oweini, J. Friedl, K. S. Tan, Y. Wang, C. L. Wong, U. Kortz, U. Stimming, and M. Srinivasan, *Chemphyschem*, 2014, **15**, 2162.
36. P. Gomez-Romero, M. Chojak, K. Cuentas-Gallegos, J. A. Asensio, P. J. Kulesza, N. Casan-Pastor and M. Lira-Cantu, *Electrochem. Commun.*, 2003, **5**, 149.
37. J. Vaillant, M. Lira-Cantu, K. Cuentas-Gallegos, N. Casan-Pastor and P. Gomez-Romero, *Prog. Solid State Chem.*, 2006, **34**, 147.
38. A. M. White and R. C. T. Slade, *Synth. Met.*, 2003, **139**, 123.
39. G. Bajwa, T. Akter and K. Lian, in *Fullerenes, Nanotubes, and Carbon Nanostructures - 219th Ecs Meeting*, ed. D. Guldi, 2011, **35**, 31.
40. G. Bajwa, Master thesis, Applied Science, University of Toronto, 2012.
41. L. Pettersson, I. Andersson, A. Selling and J. H. Grate, *Inorg. Chem.*, 1994, **33**, 982.
42. J. Arichi, M. Eternot and B. Louis, *Catal. Today*, 2008, **138**, 117.
43. K. Nomiya, K. Yagishita, Y. Nemoto and T. A. Kamataki, *J. Mol. Catal. A: Chem.*, 1997, **126**, 43.
44. R. Al-Oweini and H. El-Rassy, *J. Mol. Struct.*, 2009, **919**, 140.
45. R. Al-Oweini, B. S. Bassil, T. Palden, B. Keita, Y. H. Lan, A. K. Powell and U. Kortz, *Polyhedron*, 2013, **52**, 461.
46. R. Al-Oweini, B. S. Bassil, J. Friedl, V. Kottisch, M. Ibrahim, M. Asano, B. Keita, G. Novitchi, Y. H. Lan, A. Powell, U. Stimming and U. Kortz, *Inorg. Chem.*, 2014, **53**, 5663.
47. G. Bajwa, M. Genovese and K. Lian, *ECS J. Solid State Sci. Technol.*, 2013, **2**, M3046.
48. M. Barth, M. Lapkowski and S. Lefrant, *Electrochim. Acta*, 1999, **44**, 2117.
49. J. M. Li, K. H. Chang and C. C. Hu, *Electrochem. Commun.*, 2010, **12**, 1800.
50. J. Chen, S. L. Liu, W. Feng, G. Q. Zhang and F. L. Yang, *Phys. Chem. Chem. Phys.*, 2013, **15**, 5664.
51. I. K. Song, M. S. Kaba and M. A. Barteau, *J. Phys. Chem.*, 1996, **100**, 17528.
52. Z. Chen, V. Augustyn, J. Wen, Y. W. Zhang, M. Q. Shen, B. Dunn and Y. F. Lu, *Adv. Mater.*, 2011, **23**, 791.
53. F. Zhang, T. F. Zhang, X. Yang, L. Zhang, K. Leng, Y. Huang and Y. S. Chen, *Energ. Environ. Sci.*, 2013, **6**, 1623.
54. Tsigdino.Ga and C. J. Hallada, *Inorg. Chem.*, 1968, **7**, 437.

